

Tbx2 is essential for patterning the atrioventricular canal and for morphogenesis of the outflow tract during heart development

Zachary Harrelson¹, Robert G. Kelly¹, Sarah N. Goldin¹, Jeremy J. Gibson-Brown^{1,2,3}, Roni J. Bollag^{3,4}, Lee M. Silver³ and Virginia E. Papaioannou^{1,*}

¹Department of Genetics and Development, College of Physicians and Surgeons of Columbia University, New York, NY 10032, USA

²Department of Biology, Washington University, St Louis, MO 63130, USA

³Department of Molecular Biology, Lewis Thomas Laboratory, Princeton University, Princeton, NJ 08544, USA

⁴Institute of Molecular Genetics and Development, Medical College of Georgia, Augusta, GA 30912, USA

*Author for correspondence (e-mail: vep1@columbia.edu)

Accepted 29 July 2004

Development 131, 5041-5052
Published by The Company of Biologists 2004
doi:10.1242/dev.01378

Summary

Tbx2 is a member of the T-box transcription factor gene family, and is expressed in a variety of tissues and organs during embryogenesis. In the developing heart, *Tbx2* is expressed in the outflow tract, inner curvature, atrioventricular canal and inflow tract, corresponding to a myocardial zone that is excluded from chamber differentiation at 9.5 days post coitus (dpc). We have used targeted mutagenesis in mice to investigate *Tbx2* function. Mice heterozygous for a *Tbx2* null mutation appear normal but homozygous embryos reveal a crucial role for *Tbx2* during cardiac development. Morphological defects are observed in development of the atrioventricular canal and septation of the outflow tract. Molecular analysis reveals

that *Tbx2* is required to repress chamber differentiation in the atrioventricular canal at 9.5 dpc. Analysis of homozygous mutants also highlights a role for *Tbx2* during hindlimb digit development. Despite evidence that *TBX2* negatively regulates the cell cycle control genes *Cdkn2a*, *Cdkn2b* and *Cdkn1a* in cultured cells, there is no evidence that loss of *Tbx2* function during mouse development results in increased levels of p19^{ARF}, p16^{INK4a}, p15^{INK4b} or p21 expression in vivo, nor is there evidence for a genetic interaction between *Tbx2* and p53.

Key words: *Tbx2*, T-box, Heart development, Atrioventricular canal, Outflow tract, Cell cycle

Introduction

T-box genes encode a family of transcription factors that are molecularly and evolutionarily related by the presence of a DNA-binding T-box domain (Bollag et al., 1994). Members of the T-box gene family are found in all metazoans, ranging from hydra to humans, and are notable for the crucial roles they fulfil during embryonic development (Adell et al., 2003; Papaioannou, 2001; Showell et al., 2004). The idea that T-box genes perform crucial developmental functions stems from several observations. First, most T-box genes exhibit specific and dynamic expression profiles during embryogenesis (Papaioannou, 2001). Second, mutations in several T-box genes have been associated with genetic developmental disorders in humans (Bamshad et al., 1997; Basson et al., 1997; Braybrook et al., 2001; Lamolet et al., 2001; Yagi et al., 2003). Third, targeted mutagenesis of T-box genes in mice results in severe developmental phenotypes (Chapman and Papaioannou, 1998; Herrmann et al., 1990; Naiche and Papaioannou, 2003) that frequently model definitive aspects of related human disorders (Bruneau et al., 2001; Davenport et al., 2003; Jerome and Papaioannou, 2001; Lindsay et al., 2001).

Several T-box genes have been shown to play essential roles in heart development. At 7.5 days post coitus (dpc), the embryonic mouse heart exists as a crescent-shaped field of cells located in anterior splanchnic mesoderm. As the embryo

undergoes turning, the cardiac crescent fuses into an anteroposteriorly oriented linear heart tube. The heart tube grows and expands, and around 8.5 dpc begins a complex morphogenetic looping process that eventually brings the posterior, venous aspect of the tube to a rostral position dorsal to the outflow tract. As looping progresses through 9.5 dpc, chamber formation and septation begins such that, by 10.5 dpc, the heart has transformed from a linear tube into a four-chambered structure with prospective right and left atria and ventricles (Kaufman and Bard, 1999).

Chamber formation involves at least two important processes. First, two myocardial domains on the outer curvature of the heart tube differentiate as either an atrial or ventricular chamber. Importantly, part of the heart tube, including the outflow tract (OFT), inner curvature, atrioventricular canal (AVC) and inflow tract (IFT), escapes this developmental chamber program (Moorman and Christoffels, 2003). Simultaneously, an epithelial-to-mesenchymal transformation occurs on the inner walls of the AVC and OFT. These mesenchymal cells and their cardiac jelly matrix form two sets of opposing structures called endocardial cushions. The endocardial cushions grow, fuse, and serve as the precursors of the valves and contribute to septation. Subsequently, cardiac septation leads to division of the outflow tract into two separate outlets, and division of the atrium and

ventricle into right and left chambers (Moorman and Christoffels, 2003).

Of the six T-box genes known to be expressed in specific patterns during cardiogenesis in mouse, *Tbx1*, *Tbx2*, *Tbx3*, *Tbx5*, *Tbx18* and *Tbx20*, targeted mutagenesis has demonstrated that *Tbx1* and *Tbx5* have essential roles during cardiac development (Braybrook et al., 2001; Bruneau et al., 2001; Chapman et al., 1996; Christoffels et al., 2004; Habets et al., 2002; Hoogaars et al., 2004; Jerome and Papaioannou, 2001; Kraus et al., 2001a; Kraus et al., 2001b; Lindsay et al., 2001). Heterozygous *Tbx1* mutants display abnormal aortic arch artery remodelling, and homozygous mutants fail to septate the outflow tract (Jerome and Papaioannou, 2001; Lindsay et al., 2001). Heterozygous *Tbx5* mutants have conduction and septation defects, accompanied by reduced embryonic expression of the cardiac factor genes connexin40 (*Cx40*; *Gja5* – Mouse Genome Informatics) and natriuretic precursor peptide type A (*Nppa*, formerly known as atrial natriuretic factor or *Anf*). Homozygous *Tbx5* mutants develop hypoplastic left ventricles and atria, with altered embryonic expression of several additional cardiac factors (Bruneau et al., 2001).

Previous work has shown that *Tbx2* expression is first detected in the mouse embryo at 8.5 dpc in the allantois (Mahlapuu et al., 2001), and at 8.75 dpc in OFT, AVC and IFT myocardium (Christoffels et al., 2004; Habets et al., 2002). At 9.5 dpc, *Tbx2* is expressed in the myocardium of the OFT, inner curvature, AVC and IFT (Christoffels et al., 2004; Habets et al., 2002). A similar pattern of expression is observed in the developing chick heart (Gibson-Brown et al., 1998b; Yamada et al., 2000). Additionally, *Tbx2* is expressed at 9.5 dpc in the optic and otic vesicles, and in the naso-facial mesenchyme, and later in the developing limbs and other internal organ primordia such as the lungs and genitalia (Chapman et al., 1996; Gibson-Brown et al., 1996; Gibson-Brown et al., 1998a; Gibson-Brown et al., 1998b).

Based on the cardiac expression profile of *Tbx2*, and on evidence that *Tbx2* can act as a transcriptional repressor (Chen et al., 2004; Sinha et al., 2000), a model has been proposed whereby *Tbx2* regionalizes chamber differentiation to the prospective ventricle and atrium by repressing these programs in the OFT, inner curvature, AVC and IFT at 9.5 dpc (Christoffels et al., 2004; Habets et al., 2002). In vitro reporter assays and transgenic analyses in mice have shown that *Tbx2* can repress the transcription of *Nppa*, *Cx40* and connexin43 (*Cx43*; *Gjal* – Mouse Genome Informatics), cardiac genes whose expression is specifically restricted to the developing chambers (Chen et al., 2004; Christoffels et al., 2004; Habets et al., 2002). Additionally, transgenic embryos in which *Tbx2* is ubiquitously expressed throughout the heart tube, under the control of a β MHC promoter fragment, exhibit arrested cardiac development at looping, and a failure of chamber-specific myocardial gene expression, including *Nppa* (Christoffels et al., 2004).

An alternative, yet compatible, hypothesis suggests that *Tbx2* regulates cellular proliferation and/or survival via transcriptional repression of downstream targets, such as p19^{ARF} and p16^{INK4a} from the cyclin-dependent kinase inhibitor (*Cdkn*) 2a locus, p15^{INK4b} from *Cdkn2b*, and p21 from *Cdkn1a* (Jacobs et al., 2000; Lingbeek et al., 2002; Prince et al., 2004). A senescence bypass screen using prematurely

senescing *Bmi1*^{-/-} murine embryonic fibroblasts identified *TBX2*, with further analysis showing that senescence bypass was likely achieved by downregulation of p19^{ARF} expression and p53 protein levels. *TBX2*-expressing fibroblasts also exhibited reduced p16^{INK4a} and p15^{INK4b} transcription (Jacobs et al., 2000). Subsequent work showed that the p19^{ARF} promoter contains a functional T-box-binding element (Lingbeek et al., 2002). Others have shown that *Tbx2* can specifically regulate transcription of p21 (WAF) (Prince et al., 2004). These results, in combination with the observation that *TBX2* is amplified, and sometimes overexpressed, in a subset of primary breast tumors, breast tumor cell lines and pancreatic cancer cell lines (Barlund et al., 2000; Jacobs et al., 2000; Mahlamaki et al., 2002), has led to the hypothesis that *Tbx2* regulates cell proliferation or apoptosis through p21, p15^{INK4b}, p16^{INK4a}, and/or p19^{ARF} and p53.

We have used targeted mutagenesis of *Tbx2* in mice to gain a greater insight into the function of this gene during normal embryonic development. We engineered an ~2.2 kb deletion of the endogenous *Tbx2* locus, including part of the T-box, to generate a null allele. Mice heterozygous for the targeted locus appear normal and fertile, whereas homozygous mutant embryos exhibit lethal cardiovascular defects, revealing a crucial role for *Tbx2* during cardiac development. Abnormal expression of cardiac chamber markers *Nppa*, *Cx40* and *chisel* (*Csl*; *Smpx* – Mouse Genome Informatics) is observed in the AVC of homozygous mutants at 9.5 dpc. At 11.5-12.5 dpc, surviving homozygous mutants exhibit abnormal OFT septation and other cardiac remodeling defects, although at 9.5 dpc, markers of neural crest (NC) cells and cardiac progenitor populations contributing to the arterial pole of the heart are normally expressed. All homozygous mutants are dead by 14.5 dpc. Further studies addressing the role of *Tbx2* as a regulator of the cell cycle reveal that loss of *Tbx2* function in mouse embryos is not sufficient to deregulate cell proliferation through p21, p15^{INK4b}, p16^{INK4a}, p19^{ARF} or p53.

Materials and methods

Generating a *Tbx2* null mutation in mice

Mouse *Tbx2* genomic clones in Lambda FIXII were isolated from a 129/SvJ genomic library (Stratagene, La Jolla, CA). 2.9 kb of upstream and 6.6 kb of downstream homologous DNA sequence were ligated to a *loxP*-flanked PGK-*neo* PGK-*thymidine kinase* selection cassette, using *XbaI* and *XhoI* sites, respectively, to generate a *Tbx2*-targeting construct (Fig. 2A). The construct was designed to produce an ~2.2 kb deletion removing 207 bp of exon 1 and all of exon 2, both containing T-box coding sequence. A β -actin diphtheria toxin negative-selection cassette was placed at the 5' end of the targeting construct. A linearized targeting construct was electroporated into R1 ES cells (Nagy et al., 1993) to generate targeted cell lines. Targeting was assessed by Southern analysis on *EcoRV* genomic digests, using both 5' and 3' external probes. A targeted line was electroporated with pIC-*Cre* to remove the PGK-*neo* PGK-*thymidine kinase* cassette, resulting in the *Tbx2*^{tm1Pu} allele. Germ-line chimeras were generated by injection of targeted, *Cre*-excised ES cells into C57BL/6NTac host blastocysts.

Chimeras were mated with 129/SvEv/Tac females, to maintain the allele on an inbred background, and with C57BL/6Tac females. C57BL/6 \times 129 progeny were subsequently mated with random-bred ICR (Taconic) females. The first progeny of the chimeras were confirmed to harbor the *Tbx2*^{tm1Pu} allele by Southern analysis of *XhoI* genomic digests, using a 5' internal probe that binds a wild-type 5.1

kb fragment and a mutant 2.8 kb fragment (Fig. 2B). Subsequently, mice and embryos were genotyped by 3-primer PCR using the following primers:

- (1) 5'-CCAGCCAGGGAACATAATGAGG-3';
- (2) 5'-CTGTCCCCTGGCATTCTGG-3'; and
- (3) 5'-CCTGCAGGAATTCCTCGACC-3'.

This PCR generates a 180 bp product from the wild-type allele and an 88 bp product from the mutant allele (Fig. 2C).

Collection of embryos

The *Tbx2^{tm1Pa}* allele has been maintained both on the 129 inbred background and on a mixed (129/C57/ICR) genetic background. Heterozygous mice were intercrossed to generate homozygous mutant embryos. Embryos were dissected in phosphate-buffered saline (PBS) containing 0.2% bovine albumin (fraction V) (Sigma, St Louis, MO). Embryos for in situ hybridization and immunocytochemistry were fixed in 4% paraformaldehyde overnight, dehydrated in methanol and stored at -20°C. Embryos for histology were fixed in Bouin's fixative, dehydrated in ethanol and stored at 4°C. Yolk sacs were used for genotyping by PCR.

Histology, in situ hybridization, immunocytochemistry, and Alcian Blue staining

Embryos were collected at 10.5, 11.5 and 12.5 dpc for histology. Paraffin-embedded embryos were sectioned at 8 µm and stained with Hematoxylin and Eosin Y. In situ hybridization was performed according to previously described protocols (Wilkinson, 1992), using the following probes: mouse *Tbx2*, *Tbx3*, *Tbx5*, *Csl*, *Cx40*, *Cited1*, *MLC2v*, *βMHC*, *eHAND* and *Crabp1*; and rat *Nppa* and *Islet1*. Stained whole-mount embryos were post-fixed in 4% paraformaldehyde for vibratome sectioning. Embryos were infiltrated with 4% sucrose in PBS, 30% sucrose in PBS, and transferred to embedding mix (0.44% gelatin, 14% bovine serum albumen, 18% sucrose in PBS). Embryos were embedded in fresh embedding mix with the addition of glutaraldehyde (0.25% final concentration). Sections (50 µm) were cut on a Vibratome 1000 Plus Sectioning System (The Vibratome Company, St Louis, MO). Immunocytochemistry with rabbit anti-phospho-histone H3 primary IgG (Upstate Biotechnology, Lake Placid, NY) was performed according to standard protocols (Davis, 1993). Secondary antibody was peroxidase-conjugated goat anti-rat IgG (Jackson Immunoresearch Laboratories, West Grove, PA). Stained whole-mount embryos were post-fixed in 4% paraformaldehyde and embedded in paraffin wax for sectioning. Sections were counterstained with Nuclear Fast Red. Mitotic cells were counted in the heart tube. Alcian Blue cartilage staining was performed as previously described (Jegalian and De Robertis, 1992).

Breeding the *1v-nlacZ-24* transgene and β-galactosidase staining

Previously characterized *1v-nlacZ-24* transgenic mice (Kelly et al., 2001) were bred with *Tbx2^{tm1Pa}* heterozygous males of a mixed 129/C57/ICR background. *Tbx2^{tm1Pa}* heterozygous mice carrying the *1v-nlacZ-24* transgene were crossed with *Tbx2^{tm1Pa}* heterozygous mice to collect embryos at 9.5 and 12.5 dpc. β-Galactosidase staining was performed according to a previously described protocol (Kelly et al., 2001).

RT-PCR expression analysis

At 9.5 and 10.5 dpc, both whole embryos and a dissected trunk region including the heart were collected and stored in RNAlater RNA stabilization reagent at 4°C or -20°C (QIAGEN, Valencia, CA). RNA was extracted using RNeasy Protect Mini kit (QIAGEN, Valencia, CA), and cDNA was reverse-transcribed using SuperScript III First-Strand Synthesis System (Invitrogen Life Technologies, Carlsbad, CA). p19^{ARF}, p16^{INK4a}, p15^{INK4b} and p21 expression were assayed with semi-quantitative real-time RT-PCR performed on a DNA Engine Opticon 2 Continuous Fluorescence Detection System (MJ Research,

Waltham, MA). cDNA from adult testis was used as a positive control for p19^{ARF}, p16^{INK4a} and p15^{INK4b} expression. Mandible from a 14.5 dpc embryo was used as a positive control for p21 expression. The following primers were used for the analysis:

- (1) p19^{ARF}, p16^{INK4a}, 179 bp product, (a) 5'-GGTGGTCTTTGTG-TACCGCT-3', (b) 5'-GCCACATGCTAGACACGCTA-3';
- (2) p21, 281 bp product, (a) 5'-GTACTTCCTCTGCCCTGCTG-3', (b) 5'-CACAGAGTGAGGGCTAAGGC-3';
- (3) p15^{INK4b}, 178 bp product, (a) 5'-AGATCCCAACGCCCT-GAAC-3', (b) 5'-CTTCCTGGACACGCTTGTC-3';
- (4) Hprt, 195 bp product, (a) 5'-AGCAGTACAGCCCCAAAA-3', (b) 5'-TTTGGCTTTTCCAGTTTCA-3'.

Expression units were calculated according to the following equation:

$$(1 + \text{Eff}_R)^{\text{Ct}_R} / (1 + \text{Eff}_T)^{\text{Ct}_T} = \text{units of expression},$$

where Eff_R is efficiency of the reference PCR, Eff_T is efficiency of the target PCR, Ct_R is the cycle threshold of the reference PCR, and Ct_T is cycle threshold of the target PCR (Liu and Saint, 2002; Ramakers et al., 2003).

Results

Normal expression of *Tbx2* during early cardiogenesis, 8.5-9.5 dpc

Whole-mount in situ hybridization shows *Tbx2* expression in the cardiac crescent of 8.5 dpc mouse embryos (Fig. 1A). Vibratome sectioning of whole-mount stained embryos confirms expression in the cardiac mesoderm at 8.5 dpc (Fig. 1B). *Tbx2* expression is detected in the atrium and IFT of 8.5 dpc embryos (Fig. 1C). Hybridization of 9.5 dpc embryos reveals previously unreported areas of embryonic expression, including the septum transversum (Fig. 1D,E,H), bilateral nephrogenic mesodermal cords (intermediate mesoderm; Fig. 1D-F) and ventral body wall mesoderm caudal to the forelimbs (Fig. 1D,E). Expression is also found in pharyngeal arch mesenchyme that contains neural crest cells, including those migrating into the OFT septum (Fig. 1G). *Tbx2* is also expressed in the OFT, inner curvature, AVC and IFT of the 9.5 dpc mouse heart (Fig. 1H-L), in agreement with published expression data (Christoffels et al., 2004; Habets et al., 2002). Notably, the highest levels of cardiac expression at 9.5 dpc are found at the AVC on the outer curvature (Fig. 1K,L).

Abnormal atrioventricular morphology in *Tbx2^{tm1Pa}/Tbx2^{tm1Pa}* mutants, 9.5-10.5 dpc

To investigate the developmental functions of *Tbx2*, a targeted mutation was introduced into mice via embryonic stem (ES) cell-mediated mutagenesis. Successful targeting and Cre-mediated excision of the selection cassette generated the final *Tbx2^{tm1Pa}* allele, containing an ~2.2 kb deletion that includes the first two exons of the T-box coding sequence (Fig. 2A). The presence of this allele in mice was identified by Southern blot, PCR and sequence analysis (Fig. 2B,C).

Heterozygotes containing the *Tbx2^{tm1Pa}* allele on a mixed 129/C57/ICR background are viable, fertile, and display no obvious phenotypic abnormalities. No *Tbx2^{tm1Pa}/Tbx2^{tm1Pa}* mutants were recovered postnatally, indicating that the homozygous state is embryonic lethal (Table 1). Homozygous embryos collected between 8.5 and 18.5 dpc from heterozygous intercross matings were present at Mendelian ratios, suggesting that no homozygous mutants are lost due to

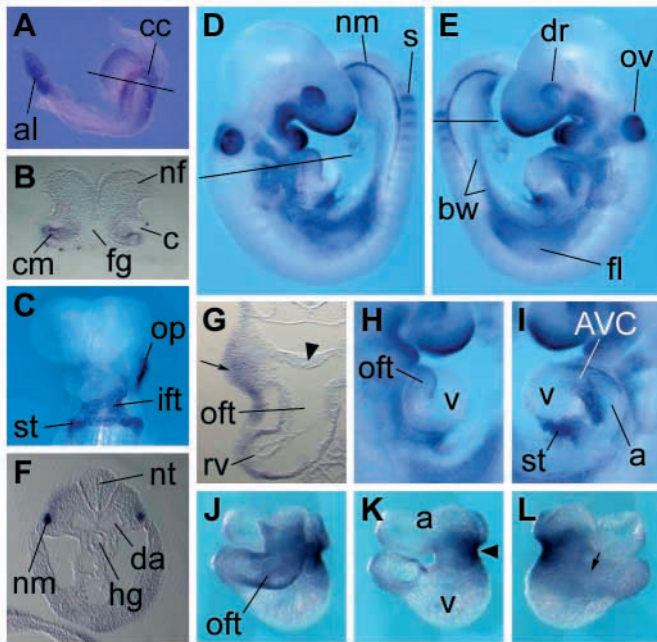


Fig. 1. *Tbx2* expression during cardiogenesis, 8.5-9.5 dpc. (A) Right view of an 8.5 dpc embryo showing *Tbx2* expression in the allantois (al) and cardiac crescent (cc). The line indicates the plane of the section shown in B. (B) Vibratome section of an 8.5 dpc embryo stained in whole-mount, showing expression in cardiac mesoderm (cm). (C) Ventral view of the head and heart of an 8.5 dpc embryo, showing *Tbx2* expression in the otic placode (op), inflow tract (ift) and septum transversum (st). (D) Right view of a 9.5 dpc embryo showing previously unreported *Tbx2* expression in somites (s) and nephrogenic mesoderm (nm). The line in the trunk indicates the plane of section in G. (E) Left view of the embryo shown in D. Labeled are the dorsal retina (dr), otic vesicle (ov), forelimb bud (fl) and previously unreported expression in the body wall of the caudal trunk and tail (bw). The line in the tail region indicates the plane of the section in F. (F) Vibratome section of a 9.5 dpc embryo showing specific expression in the nephrogenic mesoderm (nm). (G) Vibratome section of a 9.5 dpc embryo showing expression in pharyngeal arch mesenchyme (arrow), also the site of cardiac neural crest cells migrating into the outflow tract (oft). Note the absence of expression in the aorticopulmonary septum (arrowhead). (H) Right whole-mount view of a 9.5 dpc heart showing *Tbx2* expression in the outflow tract (oft). (I) Left view of the heart shown in G, demonstrating *Tbx2* expression in the atrioventricular canal (AVC) and septum transversum. (J) Ventral view of a dissected 9.5 dpc heart stained in whole-mount, showing *Tbx2* expression in the outflow tract (oft). (K) Ventral view of the heart in J with the outflow tract removed, showing *Tbx2* expression on the outer curvature of the AVC (arrowhead). (L) Dorsal view showing *Tbx2* expression in the AVC and ventricular inner curvature (arrow). nf, neural fold; c, coelom; fg, foregut; nt, neural tube; da, dorsal aorta; hg, hindgut; rv, right ventricle; v, ventricle; a, atrium.

preimplantation defects (Table 1, $\chi^2=4.85$, $P>0.05$). However, all homozygous mutants are dead by 14.5 dpc apparently due to cardiovascular insufficiency (Table 2). The mutant phenotype is first discernable at 9.5 dpc in 35% ($n=25/72$) of homozygous mutants, by the absence of a constriction at the AVC and/or an enlarged and dilated ventricle (Fig. 3A-F). At 10.5 dpc, 26% ($n=14/53$) of homozygous mutants exhibit

abnormal AVC morphology. Inflated pericardial sacs and generalized edema indicate that these embryos are suffering from circulatory distress (Fig. 3H). The hearts have undergone looping, but show the absence or reduction of an atrioventricular constriction (Fig. 3I). Transverse sections reveal that endocardial cushion development is compromised in both the AVC and OFT (Fig. 3J-O). Small endocardial cushions are observed in the OFT, which appears shortened (Fig. 3L), but cushion formation is more severely affected at the AVC, where only minor cushion-like structures from the inner curvature can be identified (Fig. 3O). Other homozygous mutants display normal cushion and atrioventricular development (Fig. 3K,N). Forty-two percent ($n=11/26$) of homozygous mutants are dead at 11.5 dpc (Table 2). Other *Tbx2*-expressing tissues are also affected: the facial region is dysmorphic with hypoplastic pharyngeal arches and the eyes have morphology equivalent to that of 9.5 dpc embryos (Fig. 3H). These phenotypic features are currently under study (Z.H. and V.E.P., unpublished).

To address whether the variability of the *Tbx2^{tm1Pa}/Tbx2^{tm1Pa}* phenotype could be attributed to the influence of genetic modifiers on the outbred background, a morphological analysis on an inbred 129 background was performed. Embryos of each genotype were present between 9.5 and 14.5 dpc at Mendelian ratios (Table 1, $\chi^2=0.0984$). Variable penetrance of a morphological atrioventricular phenotype at 10.5 dpc, and the presence of both normal and dead homozygous mutants at 12.5 dpc, suggest that genetic background plays a minimal role in affecting the range of phenotype (Table 2).

Outflow tract septation defects in *Tbx2^{tm1Pa}/Tbx2^{tm1Pa}* mutants, 11.5-12.5 dpc

Most homozygous mutants that survive to 12.5 dpc show signs of circulatory distress, including pericardial effusion and generalized edema (Fig. 4A), and all homozygous mutants are dead by 14.5 dpc (Table 2). Gross morphological analysis of dissected 12.5 dpc hearts reveals that many homozygous mutants display abnormal OFT development, such that the base of the aorta is positioned to the right of the pulmonary trunk (Fig. 4B). In wild-type embryos, the OFT becomes divided by the fusion of endocardial cushions, resulting in the formation of two separate outflow tracts exiting from specific chambers: the aorta from the left ventricle, the pulmonary trunk from the right ventricle. Histological analysis revealed that OFT septation is delayed by ~ 0.5 dpc in homozygous mutant embryos (Fig. 4D-I), and that the aortic outlet is not aligned with the left ventricle relative to normal 12.5 dpc littermates (Fig. 4J,K). Histology showed that homozygous mutants surviving to 12.5 dpc have normal atrioventricular cushion morphology (data not shown). Defects in aortic arch artery remodeling were also observed. The right 6th arch artery, which normally degenerates by 12.5 dpc, persists in half the homozygous mutants analyzed at this age ($n=3/6$) (Fig. 4L). A rightward positioned aorta and failure of the OFT to septate properly will lead to double-outlet right ventricle or other OFT anomalies that could contribute to lethality at 13.5-14.5 dpc.

Mycocardial differentiation and patterning in *Tbx2^{tm1Pa}/Tbx2^{tm1Pa}* mutants, 9.5 dpc

Whole-mount in situ hybridization was used to address the hypothesis that *Tbx2* regulates the boundaries of atrial and

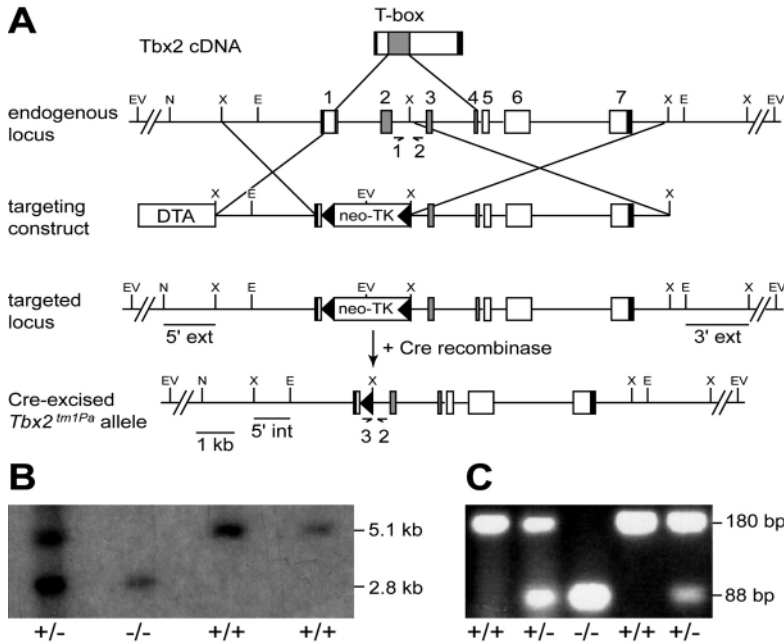


Fig. 2. Targeting strategy to generate the *Tbx2^{tm1Pa}* allele. (A) Shown are the *Tbx2* cDNA and the endogenous *Tbx2* genomic locus, where black indicates untranslated regions and gray represents the T-box coding sequence. Two hundred and seven base pairs of exon 1 and all of exon 2 were targeted for deletion with a construct containing a neomycin-thymidine kinase selection cassette (neo-TK) flanked with *loxP* sites and a negative selection diphtheria toxin element (DTA) attached at the 5' end. A targeted line was electroporated in vitro with a *Cre* recombinase gene to excise the selection cassette and generate the final *Tbx2^{tm1Pa}* allele with a ~2.2 kb deletion. (B) Southern blot analysis, with the 5' internal probe (5' int) indicated in A, confirming the presence of the *Tbx2^{tm1Pa}* allele in genomic *XhoI* digests of yolk sac DNA. The wild-type fragment is 5.1 kb, the mutant fragment is 2.8 kb. (C) PCR with the three primers indicated in A amplifies a 180 bp wild-type product and an 88 bp mutant product from yolk sac DNA. E, *EcoRI*; EV, *EcoRV*; N, *NotI*; X, *XhoI*.

ventricular development by repressing differentiation in myocardium of the OFT, inner curvature, AVC and IFT. Genes such as *Nppa*, *Csl* and *Cx40* are among the earliest differentiation markers of working atrial and ventricular myocardium, and are absent from *Tbx2*-expressing AVC myocardium of 9.5 dpc mouse hearts (Fig. 5A,C,E) (Moorman and Christoffels, 2003). *Nppa* is a hormone involved in the homeostatic regulation of blood pressure and volume in adults (Walther et al., 2002). Previous reports have shown that *Tbx2* downregulates expression of an *Nppa* reporter in transgenic mouse embryos at 10.5 dpc (Habets et al., 2002). Consistent with these results, ectopic *Nppa* expression was found in the AVC of *Tbx2^{tm1Pa}/Tbx2^{tm1Pa}* mutant embryos at 9.5 dpc ($n=4/4$) (Fig. 5B). Also, *Csl*, encoding a regulatory component of

muscle cytoskeleton (Palmer et al., 2001), was abnormally expressed in the AVC of homozygous mutants ($n=4/4$; Fig. 5D). Similar inappropriate AVC expression of *Cx40*, the gene encoding a gap junction component involved in the electrical coupling of cells and tissues (Delorme et al., 1997), was observed ($n=4/4$; Fig. 5F). *Msl1*, encoding a transcription cofactor also known as Cited1, is normally expressed in the ventricle of 9.5 dpc embryos (Fig. 5G) (Dunwoodie et al., 1998). Expression in homozygous mutants ($n=3$) ranges from normal to expanded expression in the AVC (Fig. 5H). These results suggest that the normal transcriptional program of AVC myocardium has been replaced by that of chamber myocardium.

Other markers were analyzed to assess the status of anteroposterior patterning in the heart tube and the possibility of cross-regulation between T-box genes exhibiting overlapping expression during cardiac development. The expression profile of *Tbx5*, normally within a continuous myocardial zone from the presumptive inter-ventricular boundary into the IFT (Fig. 5I) (Chapman et al., 1996; Gibson-Brown et al., 1998b), is unaffected in *Tbx2^{tm1Pa}/Tbx2^{tm1Pa}* mutants ($n=4/4$; Fig. 5J). Myosin light chain 2v (*MLC2v*; *Myl2* – Mouse Genome Informatics) is normally expressed in the OFT, ventricles and AVC at 9.5 dpc (Fig. 5K) (O'Brien et al., 1993). *MLC2v* expression is normal in homozygous mutant embryos ($n=4/4$; Fig. 5L). β -Myosin heavy chain (β MHC) expression is initially present throughout the linear heart tube but is subsequently repressed in developing atrial myocardium, such that, at 9.5 dpc, the posterior boundary of expression is found at the AVC/left atrium boundary (Fig. 5M) (Lyons et al., 1990). In *Tbx2^{tm1Pa}/Tbx2^{tm1Pa}* embryos ($n=4/4$), β MHC expression extends posterior of this border (Fig. 5N), suggesting a possible delay in transcriptional downregulation in the atrium at 9.5 dpc. The expression of *eHAND* (*Hand1* – Mouse Genome Informatics), normally observed in the left ventricle of 9.5 dpc wild-type embryos (Fig. 5O) (Thomas et al., 1998), is normal in homozygous mutants ($n=4/4$; Fig. 5P).

Table 1. Number of wild-type (+/+), heterozygous (+/-) and homozygous (-/-) *Tbx2^{tm1Pa}* embryos collected postnatally and prenatally between 8.5-18.5 dpc from heterozygous intercross matings on mixed 129/C57/ICR and pure 129 backgrounds

	Genetic background	Age (dpc)	+/+	+/-	-/-	Empty decidua
Postnatal	Mixed	3-4 weeks	38	68	0	
Prenatal	Mixed	8.5	8	6	4	0
		9.5	93	185	74	8
		10.5	51	116	53	0
		11.5	38	82	26	2
		12.5	26	66	26	1
		13.5	5	16	7	1
		14.5-18.5	21	49	28	0
Total			242	520	218	12
Total	129	9.5	8	22	9	1
		10.5	6	6	3	5
		11.5	10	18	4	1
		12.5	6	11	9	0
		14.5	1	5	4	2
				31	62	29

Table 2. Homozygous *Tbx2^{tm1Pa}* embryos from Table 1 on mixed 129/C57/ICR and pure 129 backgrounds, categorized into exclusive groups based on morphology

Genetic background	Age (dpc)	Total	Normal	Miscellaneous abnormalities	Abnormal ventricular/AV morphology	General edema*	Dead
Mixed	8.5	4	2	0	2	0	0
	9.5	72 [†]	43	4 [‡]	25	0	0
	10.5	53	38	0	14**	0	1
	11.5	26	12	2 [§]	NA	1	11
	12.5	26	6	1 [¶]	NA	5	14
	13.5	7	2	0	NA	0	5
	14.5-18.5	28	0	0	NA	0	28 ^{††}
129	9.5	9	9	0	0	0	0
	10.5	3	1	0	2	0	0
	11.5	4	1	0	NA	0	3
	12.5	9	1	0	NA	0	8
	14.5	4	0	0	NA	0	4

*Edematous in the absence of AV morphology assessment.

[†]Two of the embryos shown in Table 1 were damaged and morphology was not assessed.

[‡]Two unturned littermates with disorganized tissue mass ventral to head folds, one grossly retarded embryo, and one embryo with abnormal eye morphology only.

[§]One embryo with hypoplastic face, the other embryo with hypoplastic face, open neural folds and abnormal hindlimb.

[¶]One embryo with hypoplastic jaw.

**Embryos also edematous.

^{††}Three dead embryos collected at 14.5 dpc had bilateral hindlimb-specific duplications of digit IV.

NA, not applicable, AV morphology not assessed.

Tbx3 expression in the AVC was also assessed and was found to be unaffected in homozygous mutants (data not shown).

Further expression analysis addressed possible explanations for the OFT defects observed in *Tbx2^{tm1Pa}/Tbx2^{tm1Pa}* mutants at 12.5 dpc. Cellular retinoic acid binding protein 1 (*Crabp1*) is a NC marker gene normally expressed in dorsal-ventral stripes between the neural tube and the pharyngeal arches at 9.5 dpc (Fig. 5Q) (Giguere et al., 1990). *Crabp1* expression is normal in *Tbx2^{tm1Pa}/Tbx2^{tm1Pa}* mutants ($n=4/4$; Fig. 5R). A population of splanchnic mesoderm that will contribute to myocardium at both poles of the heart, including the OFT and right ventricle (RV), is marked by expression of the LIM homeobox gene *Islet1* at 9.5 dpc (Fig. 5S) (Cai et al., 2003). Homozygous mutant embryos have normal *Islet1* expression ($n=4/4$; Fig. 5T). The *Fgf10* enhancer-trap transgene *lv-nlacZ-24* was bred onto the mutant background to assess the integrity of the anterior heart field (AHF) in *Tbx2^{tm1Pa}/Tbx2^{tm1Pa}* embryos (Kelly et al., 2001). The transgene was normally expressed in RV and OFT myocardium, and pharyngeal arch mesoderm, in 9.5 dpc homozygous mutant ($n=7/7$) and heterozygous control embryos (Fig. 5U,V). Transgenic homozygous mutant embryos at 12.5 dpc confirm a normal contribution of the AHF to the RV and OFT ($n=3/3$) (Fig. 5W,X).

Myocardial cell proliferation in *Tbx2^{tm1Pa}/Tbx2^{tm1Pa}* mutants, 9.5 dpc

Immunocytochemistry with an anti-phospho-histone H3 antibody was used to assay cell proliferation in 9.5 dpc embryos. Whole-mount staining showed no differences in the global pattern of phospho-histone H3-positive cells between wild-type ($n=2$) and homozygous mutant ($n=3$) embryos. Cell counts in the entire myocardium showed no difference in the percentage of phospho-histone H3-positive cells between wild-type (1.97%, $n=17,738$ cells) and homozygous mutant populations (1.89%, $n=28,155$ cells; $\chi^2=0.87$,

$P>0.05$), demonstrating normal cell proliferation levels in *Tbx2^{tm1Pa}/Tbx2^{tm1Pa}* hearts at 9.5 dpc.

Digit duplication in *Tbx2^{tm1Pa}/Tbx2^{tm1Pa}* mutants at 14.5 dpc

In the most developmentally advanced homozygous mutant embryos recovered, a bilateral, hindlimb-specific, digit IV duplication was observed ($n=3/3$ embryos; Fig. 6A,B). Alcian Blue staining showed two cartilage condensations within the first phalangeal segment of digit IV ($n=4/4$ hindlimbs; Fig. 6C). *Tbx2* expression has been reported in the interdigital mesenchyme between digits IV and V at 13.5 dpc (Gibson-Brown et al., 1996).

Normal p21, p19^{ARF}, p16^{INK4a} and p15^{INK4b} expression and p53 function in *Tbx2^{tm1Pa}/Tbx2^{tm1Pa}* mutants, 9.5-10.5 dpc

A growing body of work suggests that *Tbx2* can inhibit cell cycle arrest and/or apoptosis by directly repressing p19^{ARF} transcription, which then leads to the repression of p53 activity (Jacobs et al., 2000; Lingbeek et al., 2002). p53 exerts its effects on cellular proliferation/survival through multiple downstream targets, including p21, although many of these factors also regulate the cell cycle via p53-independent pathways (Taylor and Stark, 2001). Recent work has led to the hypothesis that *Tbx2* can also regulate proliferation/survival through a p19^{ARF}-p53-independent p21 pathway (Prince et al., 2004). *TBX2* expression has also been shown to downregulate p16^{INK4a} and p15^{INK4b} transcription in cultured cells (Jacobs et al., 2000). Semi-quantitative real-time RT-PCR was used to analyze p21, p19^{ARF}, p16^{INK4a} and p15^{INK4b} expression levels in homozygous mutant versus wild-type or heterozygous embryos. Normal p21 expression levels were observed in whole 9.5 dpc ($n=2$) and 10.5 dpc ($n=3$) homozygous mutants, and also in a dissected trunk region including the heart from

10.5 dpc homozygous mutants ($n=3$; Fig. 7A). One primer pair was designed to detect the combined expression of p19^{ARF} and p16^{INK4a} expression, which is normally undetectable in wild-type embryos (Zindy et al., 1997). No evidence of upregulated p19^{ARF}+p16^{INK4a} expression was found in whole 9.5 dpc ($n=3$) or 10.5 dpc ($n=4$) homozygous mutants, or in a dissected trunk region including the heart from 10.5 dpc homozygous mutants ($n=4$; Fig. 7B). No evidence of p15^{INK4b} expression, also undetectable in wild-type embryos (Zindy et al., 1997), was found in whole 9.5 dpc ($n=4$) or 10.5 dpc ($n=4$) homozygous mutants, or in a dissected trunk region including the heart from 10.5 dpc homozygous mutants ($n=4$; Fig. 7C). These results indicate that loss of *Tbx2* function is not sufficient to upregulate the expression of p21, p19^{ARF}, p16^{INK4a} or p15^{INK4b} in 9.5-10.5 dpc mouse embryos.

A potential genetic interaction between *Tbx2* and p53 (*Trp53*) was investigated by a morphological analysis of *Tbx2*

Trp53/Tbx2 Trp53 double homozygous mutants. *Tbx2^{tm1Pa}* heterozygotes on a mixed background were crossed with homozygous 129-*Trp53^{tm1Tsj}* mutants (Jacks et al., 1994). If the *Tbx2^{tm1Pa}/Tbx2^{tm1Pa}* phenotype were due to upregulated p53 function, the prediction would be that this phenotype should be rescued in double homozygous mutants. At 10.5 dpc, double homozygous mutants ($n=3/8$) are edematous with inflated pericardial sacs, dysmorphic faces, hypoplastic arches and delayed optic morphology, similar to *Tbx2^{tm1Pa}/Tbx2^{tm1Pa}* mutants, and at 11.5-12.5 dpc ($n=6/8$), double homozygous mutants are dead. The similar range of phenotype and time of death among *Tbx2^{tm1Pa} Trp53^{tm1Tsj}/Tbx2^{tm1Pa} Trp53^{tm1Tsj}* mutants and *Tbx2^{tm1Pa}/Tbx2^{tm1Pa}* mutants suggests that there is no major developmental genetic interaction between *Tbx2* and p53.

Discussion

Tbx2, *Tbx5* and heart chamber differentiation

To address the developmental functions of *Tbx2*, we have used targeted mutagenesis in mice to produce a ~2.2 kb deletion in the endogenous *Tbx2* locus, including sequence encoding part of the DNA-binding T-box domain. Our results show that heterozygotes are viable, fertile, and grossly normal, but that homozygous mutants die between 10.5 and 14.5 dpc because of cardiac insufficiency. A quarter of homozygous mutants dissected at 10.5 dpc exhibit signs of circulatory distress, including inflated pericardial sacs and generalized edema, and approximately 40% are dead by 11.5 dpc; the rest are dead by 14.5 dpc. Histological analysis of 10.5 dpc homozygous mutants shows the presence of distinct ventricular and atrial myocardial morphologies, but deficient endocardial cushion formation in the AVC. Importantly, the first observable defect in homozygous mutants presents as abnormal morphology at the AVC and/or left ventricle at 9.5 dpc, a day before the circulatory distress surfaces.

The cardiac phenotype of *Tbx5* homozygous null mutant mice (Bruneau et al., 2001), in vitro reporter assays, and

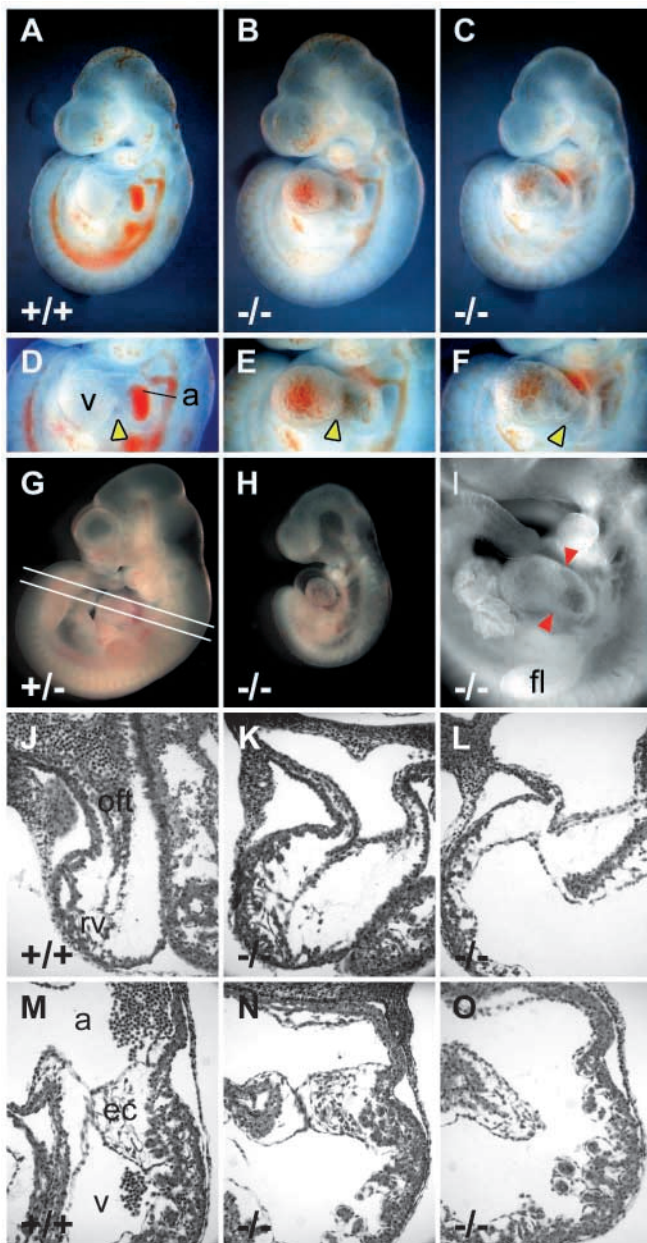


Fig. 3. Abnormal atrioventricular morphology in *Tbx2^{tm1Pa}/Tbx2^{tm1Pa}* mutants ($-/-$), 9.5-10.5 dpc. (A-C) Left views of a wild-type embryo (A, $+/+$) and two homozygous mutants (B,C) with abnormal atrioventricular (AV) morphology at 9.5 dpc. (D-F) Enlarged images highlight the AV canal that in wild type is distinguishable by the presence of a morphological constriction, indicated with the yellow arrowhead (D). Homozygous mutants frequently lack this AV constriction (E) or exhibit an enlarged or dilated ventricle (F). Left views of a (G) normal heterozygous embryo and a (H) homozygous mutant at 10.5 dpc. White lines in G indicate the planes of section for histology in J-O. The homozygous embryo in H shows signs of circulatory distress. (I) Closer inspection of another affected homozygous mutant shows a lack of constriction at the AV canal (red arrowheads). (J-L) Transverse histology at the outflow tract (OFT) of wild-type and homozygous mutant embryos at 10.5 dpc. Homozygous mutants that appear morphologically normal by external criteria show normal OFT endocardial cushion development (K). Distressed homozygous mutants have small endocardial cushions and the OFT appears to be shortened (L). (M-O) Transverse histology at the AV canal of the same embryos shown in J-L. Some homozygous mutants have normal endocardial cushion formation (N). Distressed homozygous mutants show compromised cushion formation (O). v, ventricle; a, atrium; ofl, outflow tract; rv, right ventricle; ec, endocardial cushion.

transgenic analysis of the regulation of the chamber-specific gene *Nppa* (Christoffels et al., 2004; Habets et al., 2002) have culminated in the following hypothesis regarding the development of chamber myocardium in the 9.5 dpc mouse heart: *Tbx5* activates a chamber differentiation program and *Tbx2* spatially restricts this program by repressing a set of downstream target genes in non-chamber myocardium of the AVC and OFT. *Tbx5* homozygous mutants exhibit reduced expression of at least two chamber-specific genes, *Nppa* and *Cx40* (Bruneau et al., 2001). Biochemical evidence has shown that *Tbx5* and *Nkx2.5* can specifically and cooperatively bind the promoter of *Nppa*, synergistically activating reporter expression (Hiroi et al., 2001). *Nkx2.5* is a homeodomain transcription factor that is one of the earliest markers of the mouse cardiac lineage and interacts with a number of factors in the cooperative regulation of downstream targets (Bruneau et al., 2000). *Nkx2.5* homozygous mutants display reduced expression of a number of cardiac genes, including *Nppa* (Tanaka et al., 1999). Biochemical experiments have shown that *Tbx2* also has the capacity to specifically regulate *Nppa* in cooperation with *Nkx2.5* and that this interaction is preferred in competitive binding assays between *Tbx2*, *Tbx5* and *Nkx2.5* (Habets et al., 2002). *Tbx2* can also specifically regulate the expression of other chamber-specific genes, including *Cx40* (Christoffels et al., 2004).

The embryonic expression profile of *Tbx2*, and both the

morphological and molecular aspects of the *Tbx2* homozygous mutant phenotype, support a model in which *Tbx2*-mediated repression localizes chamber differentiation to the prospective ventricle and atrium at 9.5 dpc. Whole-mount in situ hybridization data confirm previously reported results that *Tbx2* is normally expressed in myocardium of the OFT, inner curvature, AVC and IFT of the 9.5 dpc mouse heart (Christoffels et al., 2004; Habets et al., 2002). While AVC morphology is normal in a subset of *Tbx2^{tm1Pa}/Tbx2^{tm1Pa}* mutants, all homozygous mutants exhibit ectopic expression of the chamber-specific markers analyzed: *Nppa*, *Csl*, *Cx40* and *Cited1*. Importantly, there is no evidence that *Tbx2* directly affects anteroposterior patterning of the heart tube, as the posterior expression boundaries of *MLC2v* and *eHAND* are unaffected in homozygous mutants. Loss of *Tbx2*, however, can affect the expression pattern of some genes, such as β MHC, which fails to be downregulated in *Tbx2^{tm1Pa}/Tbx2^{tm1Pa}* atria.

The abnormal development of the AVC provides a plausible explanation for the lethality observed amongst *Tbx2^{tm1Pa}/Tbx2^{tm1Pa}* mutants at 10.5–11.5 dpc. Insulation of the ventricular and atrial chambers by a distinct myocardial zone is crucial for the mechanical and electrical isolation of chambers that are functionally separate in the mature heart. The molecular characterization described above suggests that *Tbx2^{tm1Pa}/Tbx2^{tm1Pa}* hearts are developing atrial and ventricular

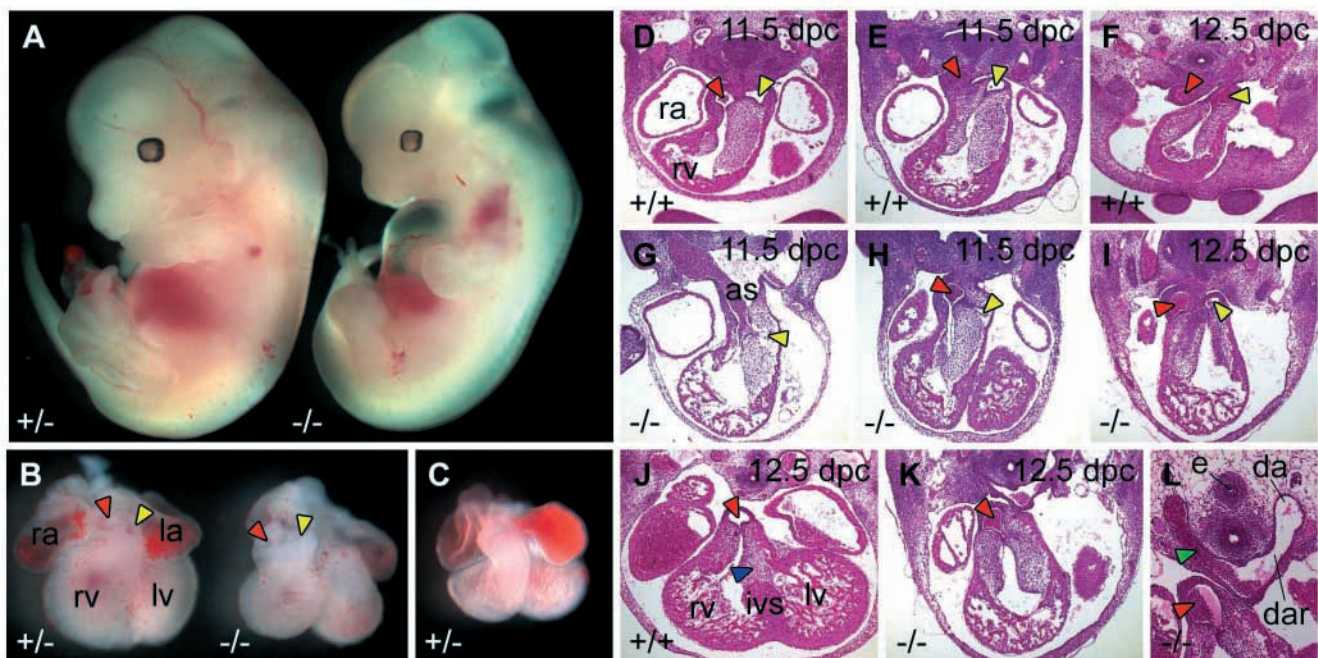


Fig. 4. Outflow tract septation defects in *Tbx2^{tm1Pa}/Tbx2^{tm1Pa}* homozygous mutants ($-/-$), 11.5–12.5 dpc. (A) Left views of a normal heterozygote ($+/-$) and a homozygous mutant embryo. The mutant is suffering from circulatory distress. (B,C) Ventral view of hearts from the 12.5 dpc embryos in A (B) and a normal heterozygous 11.5 dpc heart (C) for comparison. The 12.5 dpc homozygous mutant aorta (red arrowhead) is abnormally positioned to the right relative to the pulmonary trunk (yellow arrowhead). (D–I) Transverse histology of wild-type (D–F, $+/+$) and homozygous mutant embryos (G–I) over a range of stages between 11.5 and 12.5 dpc. Homozygous mutant histology shows delayed outflow tract (OFT) septation into separate aortic (red arrowheads) and pulmonary (yellow arrowheads) outlets. (J,K) Transverse histology from 12.5 dpc wild-type (J) and homozygous mutant embryos (K). Homozygous mutants frequently show a misalignment where the aortic outlet is abnormally positioned with respect to the left ventricle. Normally at 12.5 dpc the aortic outlet is situated near the left ventricle, separated only by endocardial cushion (blue arrowhead in J). (L) The right 6th arch artery (green arrowhead) is often persistent in 12.5 dpc homozygous mutant embryos. ra, right atrium; la, left atrium; rv, right ventricle; lv, left ventricle; as, aortic sac; e, esophagus; da, descending aorta; dar, ductus arteriosus.

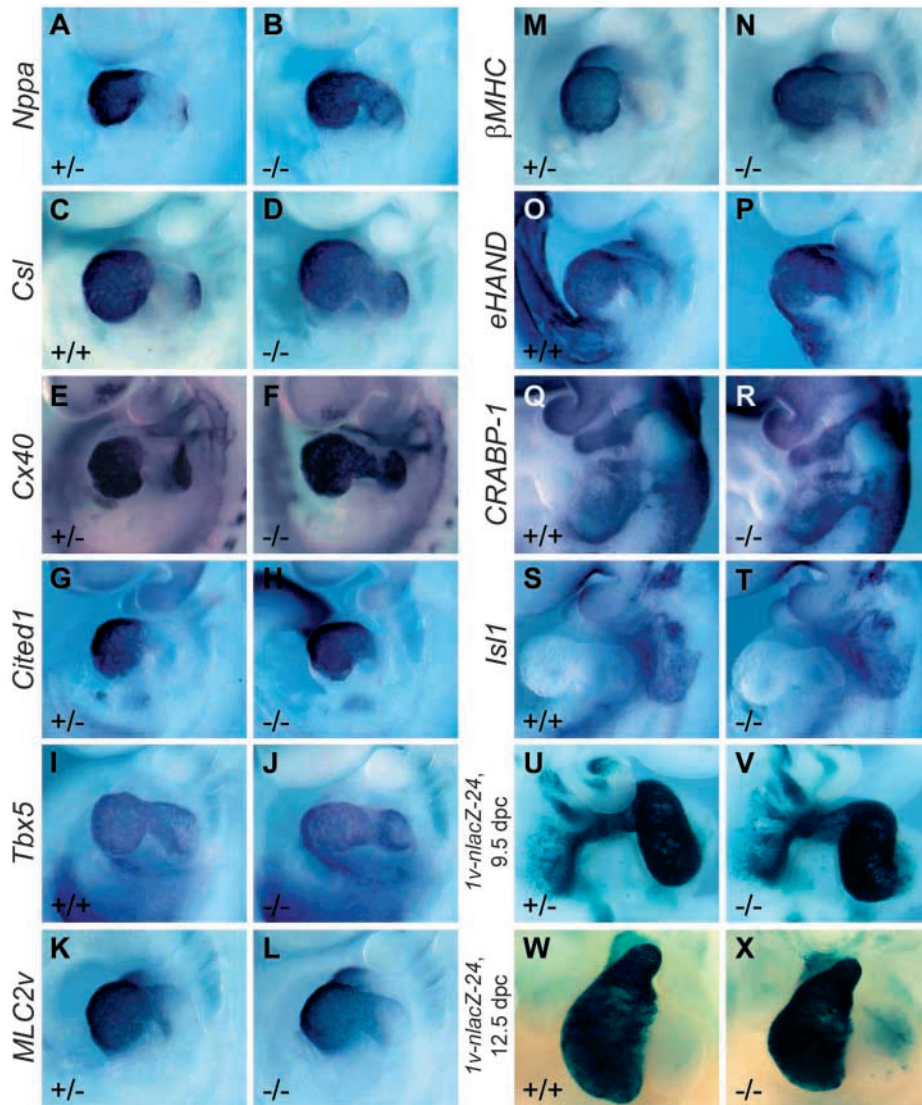


Fig. 5. Chamber differentiation in the myocardium of the AVC in *Tbx2^{tm1Pa/Tbx2^{tm1Pa}}* mutants (-/-), 9.5 dpc. Various gene expression patterns in normal wild-type (+/+) or heterozygous (+/-) embryos (A,C,E,G,I,K,M,O,Q,S,U,W) compared with homozygous mutants (B,D,F,H,J,L,N,P,R,T,V,X). *Nppa* is ectopically expressed in myocardium at the atrioventricular canal (AVC) in homozygous mutants (B), as is *Csl* (D) and *Cx40* (F). Some homozygous mutant embryos have an extended domain of *Cited1* expression into the AVC (H). *Tbx5* expression at the AVC is normal in homozygous mutants (J). *MLC2v* expression is normal (L), but abnormal atrial expression of β MHC (N) is observed in homozygous mutants. *eHAND* expression is normal in homozygous mutants (P). Neural crest cell *Crabp1* expression is normal in homozygous mutants (R). Expression of *Islet1* and the *Fgf10* enhancer-trap transgene *1v-nlacZ-24* are normal in 9.5 dpc homozygous mutants (T,V). *1v-nlacZ-24* expression is also normal in homozygous mutants at 12.5 dpc.

chambers whose conduction and contraction are coupled. The lack of functional separation between the developing chambers could explain the lethal cardiac distress that kills many homozygous mutants.

***Tbx2* and remodeling of the outflow tract**

Many *Tbx2^{tm1Pa/Tbx2^{tm1Pa}}* embryos escape the cardiac distress imposed by ectopic chamber differentiation in the AVC at 9.5 dpc. Of those that survive, however, many experience similar

distress by 12.5 dpc. The homozygous mutant population displays a range of defects in septation and remodeling of the OFT and aortic arch arteries. Histological analysis indicates misalignment of the aorta and pulmonary trunk with the appropriate ventricles. Although interventricular septum formation is still incomplete by 12.5 dpc, persistence of such misalignment will eventually result in double-outlet right ventricle, where both the aorta and pulmonary trunk emerge from the right ventricle. There are several possible

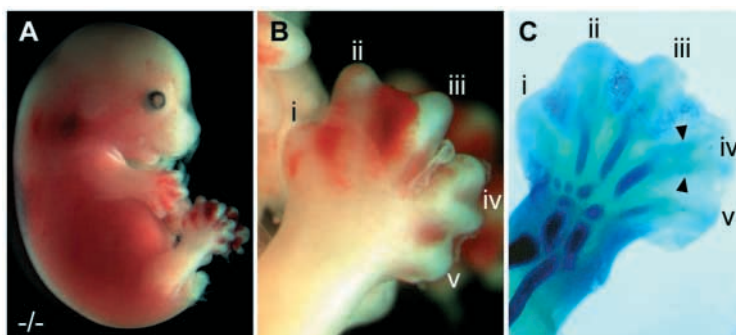


Fig. 6. Hindlimb-specific, bilateral distal digit duplication in *Tbx2^{tm1Pa/Tbx2^{tm1Pa}}* mutants (-/-). (A) Right view of a dead homozygous mutant embryo (with tail removed) collected at 14.5 dpc. (B) High magnification view of the embryo in A showing a distal duplication of digit IV in the hindlimb. (C) Dorsal view of an Alcian Blue-stained right hindlimb from a dead embryo dissected at 14.5 dpc, showing duplicated cartilage condensations (arrowheads) within the first phalangeal segment of digit IV.

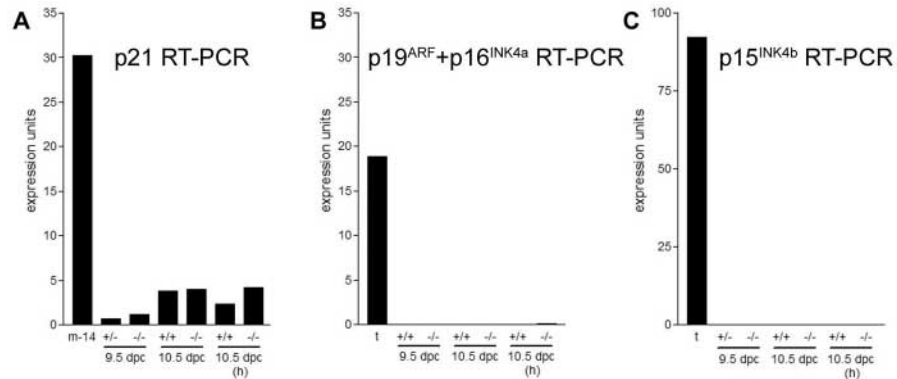


Fig. 7. Normal levels of p21, p19^{ARF}, p16^{INK4a} and p15^{INK4b} expression in *Tbx2*^{tm1Pa}/*Tbx2*^{tm1Pa} mutants (–/–), 9.5–10.5 dpc. (A) Results of semi-quantitative RT-PCR expression analysis demonstrating no evidence of elevated p21 transcription in homozygous mutants versus either wild-type (+/+) or heterozygous (+/–) controls at 9.5 dpc, 10.5 dpc, or in cases with dissected 10.5 dpc heart and trunk (h). Mandible from a 14.5 dpc mouse embryo (m-14) serves as the positive control. (B) Results of semi-quantitative RT-PCR expression analysis demonstrating no evidence of elevated p19^{ARF} or p16^{INK4a} transcription in homozygous mutants versus wild-type controls at 9.5 dpc, 10.5 dpc or in cases with dissected 10.5 dpc heart and trunk (h). Adult testis (t) serves as the positive control. (C) Results of semi-quantitative RT-PCR expression analysis demonstrating no evidence of elevated p15^{INK4b} transcription in homozygous mutants versus either wild-type or heterozygous controls at 9.5 dpc, 10.5 dpc, or in cases with dissected 10.5 dpc heart and trunk (h). Adult testis (t) serves as the positive control.

explanations for the defects observed in 12.5 dpc *Tbx2*^{tm1Pa}/*Tbx2*^{tm1Pa} mutants. First, the defects may be due to misalignment of the OFT and the ventricles, as a secondary consequence of torsional strains on looping imposed by abnormal AVC development. Another possibility is that homozygous mutants surviving to 12.5 dpc experience primary defects in the elongation, septation and rotation of the OFT, such that the ventricular outlets never achieve their final alignment. The fact that *Tbx2* is expressed in the OFT from 8.75 dpc until late fetal stages supports the latter hypothesis (Fig. 1G,I) (Christoffels et al., 2004). However, normal expression of *Islet1* and the *Fgf10* enhancer-trap *1v-nlacZ-24* transgene suggests that the population of cells contributing the majority of myocardium to the OFT and RV are present and normal in *Tbx2*^{tm1Pa}/*Tbx2*^{tm1Pa} mutants. A third possibility is that *Tbx2* is required in the cardiac NC for OFT septation, or that *Tbx2* targets regulate NC deployment during septation and aortic arch artery remodelling (Kirby and Waldo, 1995), although normal *Crabp1* expression in homozygous mutant embryos at 9.5 dpc provides preliminary evidence against this hypothesis. Conditional mutagenesis experiments will be required to resolve this issue.

***Tbx2* and the developing limbs**

Few *Tbx2*^{tm1Pa}/*Tbx2*^{tm1Pa} embryos survive past 13.5 dpc, but those that do display bilateral, hindlimb-specific, distal digit IV duplications, revealing a late role for the gene during patterning of the hindlimb autopod. *Tbx2* is expressed in the interdigital mesenchyme between developing digits IV and V of 13.5 dpc mouse embryos (Gibson-Brown et al., 1996), and our observations could be compatible with the involvement of *Tbx2* in regulating apoptosis in this region. Recent work has implicated *Tbx2* as a posteriorizing influence during digit identity specification in chick and mouse (Suzuki et al., 2004). Our results, however, do not address this possible role for *Tbx2*. Further work will be required before the exact role of *Tbx2* during limb patterning and digit specification is understood.

***Tbx2* and the cell cycle**

Despite overwhelming evidence connecting *Tbx2* to the cell cycle (Barlund et al., 2000; Jacobs et al., 2000; Lingbeek et al., 2002; Mahlamaki et al., 2002; Prince et al., 2004), *Tbx2*^{tm1Pa}/*Tbx2*^{tm1Pa} embryos offer no evidence that any of the implicated pathways are dysregulated during embryogenesis. There is no difference in p19^{ARF}, p16^{INK4a}, p15^{INK4b} or p21 expression levels between wild-type embryos and homozygous mutants at 9.5 or 10.5 dpc, as assessed by semi-quantitative RT-PCR. Additionally, introduction of the *Trp53*^{tm1Tyj} mutation into the *Tbx2*^{tm1Pa} line failed to rescue the morphological range or presentation of the *Tbx2*^{tm1Pa}/*Tbx2*^{tm1Pa} phenotype, eliminating the possibility of a specific genetic interaction. Loss of *Tbx2* function is therefore not sufficient to upregulate expression of p19^{ARF}, p16^{INK4a}, p15^{INK4b} or p21 in 9.5–10.5 dpc mouse embryos, nor can the *Tbx2*^{tm1Pa}/*Tbx2*^{tm1Pa} phenotype be attributed to an excess of p53.

Although *Tbx2*^{tm1Pa}/*Tbx2*^{tm1Pa} embryos do not exhibit precocious p19^{ARF}, p16^{INK4a}, p15^{INK4b} or p21 expression, or abnormal p53 function, these findings do not rule out a role for *Tbx2* in regulating the cell cycle. The knowledge that *TBX2* is capable of regulating p19^{ARF}, p16^{INK4a}, p15^{INK4b} and p21 expression in vitro (Lingbeek et al., 2002; Prince et al., 2004), and that *TBX2*-mediated regulation of p19^{ARF} has an observable biological effect on cellular senescence (Jacobs et al., 2000), combined with the lack of a cell cycle phenotype in 9.5–10.5 dpc *Tbx2*^{tm1Pa}/*Tbx2*^{tm1Pa} mutants, suggests that compensating factors may participate in the regulation of this pathway. *Tbx3* is the most obvious candidate for several reasons. Within the T-box family, *Tbx2* and *Tbx3* are more closely related to each other than to any other family member, and both can function as transcriptional repressors (Agulnik et al., 1996; Carlson et al., 2001; Sinha et al., 2000). *Tbx2* and *Tbx3* exhibit extensive expression overlap in many tissues during mouse development, including the AVC and the limbs (Chapman et al., 1996; Christoffels et al., 2004; Gibson-Brown et al., 1996; Hoogaars et al., 2004). *Tbx3* has also been

implicated in p19^{ARF}-mediated regulation of the cell cycle and cell death (Carlson et al., 2002; Lingbeek et al., 2002). Therefore, the likely functional overlap between *Tbx2* and *Tbx3* may account for our observations that p19^{ARF}, p16^{INK4a}, p15^{INK4b} and p21 expression, and p53 function, are normal in *Tbx2^{tm1Pa}/Tbx2^{tm1Pa}* mutants at 9.5–10.5 dpc. We have initiated an analysis of *Tbx2*, *Tbx3* double mutants to investigate potential functional overlap, particularly with respect to cardiac development and cell cycle regulation.

We thank members of the Papaioannou Laboratory for support and helpful criticism. We thank V. Christoffels and A. Moorman for discussion and the exchange of ideas. We also thank Carl de Luca for discussion and assistance performing RT-PCR. Probes were generously donated by V. Christoffels, R. Harvey, L. Micquerol, S. Dunwoodie and D. Srivastava. This work was supported by NIH grants HD20275 (L.M.S.) and HD33082 (V.E.P.). R.G.K. is an INSERM Research Fellow.

References

- Adell, T., Grebenjuk, V. A., Wiens, M. and Muller, W. E. G. (2003). Isolation and characterization of two T-box genes from sponges, the phylogenetically oldest metazoan taxon. *Dev. Genes Evol.* **213**, 421–434.
- Agulnik, S. I., Garvey, N., Hancock, S., Ruvinsky, I., Chapman, D. L., Agulnik, I., Bollag, R., Papaioannou, V. and Silver, L. M. (1996). Evolution of mouse *T-box* genes by tandem duplication and cluster dispersion. *Genetics* **144**, 249–254.
- Bamshad, M., Lin, R. C., Law, D. J., Watkins, W. S., Krakowiak, P. A., Moore, M. E., Franceschini, P., Lala, R., Holmes, L. B., Gebuhr, T. C. et al. (1997). Mutations in human *TBX3* alter limb, apocrine and genital development in ulnar-mammary syndrome. *Nat. Genet.* **16**, 311–315.
- Barlund, M., Monni, O., Kononen, J., Cornelison, R., Torhorst, J., Sauter, G., Kallioniemi, O.-P. and Kallioniemi, A. (2000). Multiple genes at 17q23 undergo amplification and overexpression in breast cancer. *Cancer Res.* **60**, 5340–5344.
- Basson, C. T., Bachinsky, D. R., Lin, R. C., Levi, T., Elkins, J. A., Soultz, J., Grayzel, D., Kroumpouzou, E., Traill, T. A., Leblanc-Straceski, J. et al. (1997). Mutations in human cause limb and cardiac malformation in Holt-Oram syndrome. *Nat. Genet.* **15**, 30–35.
- Bollag, R. J., Siegfried, Z., Cebra-Thomas, J. A., Garvey, N., Davison, E. M. and Silver, L. M. (1994). An ancient family of embryonically expressed mouse genes sharing a conserved protein motif with the *T* locus. *Nat. Genet.* **7**, 383–389.
- Braybrook, C., Doudney, K., Marcano, A. C. B., Arnason, A., Bjornsson, A., Patton, M. A., Goodfellow, P. J., Moore, G. E. and Stanier, P. (2001). The T-box transcription factor gene *TBX22* is mutated in X-linked cleft palate and ankyloglossia. *Nat. Genet.* **29**, 179–183.
- Bruneau, B. G., Bao, Z.-Z., Tanaka, M., Schott, J.-J., Izumo, S., Cepko, C. L., Seidman, J. G. and Seidman, C. E. (2000). Cardiac expression of the ventricle-specific homeobox gene *Irx4* is modulated by Nkx2-5 and dHand. *Dev. Biol.* **217**, 266–277.
- Bruneau, B. G., Nemer, G., Schmitt, J. P., Charron, F., Robitaille, L., Caron, S., Conner, D. A., Gessler, M., Nemer, M., Seidman, C. E. et al. (2001). A murine model of Holt-Oram syndrome defines roles of the T-box transcription factor *Tbx5* in cardiogenesis and disease. *Cell* **106**, 709–721.
- Cai, C.-L., Liang, X., Shi, Y., Chu, P.-H., Pfaff, S. L., Chen, J. and Evans, S. (2003). Isl1 identifies a cardiac progenitor population that proliferates prior to differentiation and contributes a majority of cells to the heart. *Dev. Cell* **5**, 877–889.
- Carlson, H., Ota, S., Campbell, C. E. and Hurlin, P. J. (2001). A dominant repression domain in *Tbx3* mediates transcriptional repression and cell immortalization: relevance to mutations in *Tbx3* that cause ulnar-mammary syndrome. *Hum. Mol. Genet.* **10**, 2403–2413.
- Carlson, H., Ota, S., Song, Y., Chen, Y. and Hurlin, P. J. (2002). *Tbx3* impinges on the p53 pathway to suppress apoptosis, facilitate cell transformation and block myogenic differentiation. *Oncogene* **21**, 3827–3835.
- Chapman, D. L. and Papaioannou, V. E. (1998). Three neural tubes in mouse embryos with mutations in the T-box gene *Tbx6*. *Nature* **391**, 695–697.
- Chapman, D. L., Garvey, N., Hancock, S., Alexiou, M., Agulnik, S. I., Gibson-Brown, J. J., Cebra-Thomas, J., Bollag, R. J., Silver, L. M. and Papaioannou, V. E. (1996). Expression of the T-box family genes, *Tbx1-Tbx5*, during early mouse development. *Dev. Dyn.* **206**, 379–390.
- Chen, J. R., Chatterjee, B., Meyer, R., Yu, J. C., Borke, J. L., Isaacs, C. M., Kirby, M. L., Lo, C. W. and Bollag, R. J. (2004). *Tbx2* represses expression of Connexin43 in osteoblastic-like cells. *Calcif. Tissue Int.* **74**, 561–573.
- Christoffels, V. M., Hoogaars, W. M. H., Tessari, A., Clout, D. E. W., Moorman, A. F. M. and Campione, M. (2004). T-Box transcription factor *Tbx2* represses differentiation and formation of the cardiac chambers. *Dev. Dyn.* **229**, 763–770.
- Davenport, T. G., Jerome-Majewska, L. A. and Papaioannou, V. E. (2003). Mammary gland, limb and yolk sac defects in mice lacking *Tbx3*, the gene mutated in human ulnar mammary syndrome. *Development* **130**, 2263–2273.
- Davis, C. A. (1993). Whole-mount immunohistochemistry. *Methods Enzymol.* **225**, 502–516.
- Delorme, B., Dahl, E., Jarry-Guichard, T., Briand, J.-P., Willecke, K., Gros, D. and Theveniau-Ruissy, M. (1997). Expression pattern of connexin gene products at the early developmental stages of the mouse cardiovascular system. *Circ. Res.* **81**, 423–437.
- Dunwoodie, S. L., Rodriguez, T. A. and Beddington, R. S. P. (1998). *Msg1* and *Mrg1*, founding members of a gene family, show distinct patterns of gene expression during mouse embryogenesis. *Mech. Dev.* **72**, 27–40.
- Gibson-Brown, J. J., Agulnik, S. I., Chapman, D. L., Alexiou, M., Garvey, N., Silver, L. M. and Papaioannou, V. E. (1996). Evidence of a role for T-box genes in the evolution of limb morphogenesis and the specification of forelimb/hindlimb identity. *Mech. Dev.* **73**, 93–101.
- Gibson-Brown, J. J., Agulnik, S. I., Silver, L. M., Niswander, L. and Papaioannou, V. E. (1998a). Involvement of T-box genes *Tbx2-Tbx5* in vertebrate limb specification and development. *Development* **125**, 2499–2509.
- Gibson-Brown, J. J., Agulnik, S. I., Silver, L. M. and Papaioannou, V. E. (1998b). Expression of T-box genes *Tbx2-Tbx5* during chick organogenesis. *Mech. Dev.* **74**, 165–169.
- Giguere, V., Lyn, S., Yip, P., Siu, C.-H. and Amin, S. (1990). Molecular cloning of cDNA encoding a second cellular retinoic acid-binding protein. *Proc. Natl. Acad. Sci. USA* **87**, 6233–6237.
- Habets, P. E. M. H., Moorman, A. F. M., Clout, D. E. W., van Roon, M. A., Lingbeek, M., van Lohuizen, M., Campione, M. and Christoffels, V. M. (2002). Cooperative action of *Tbx2* and *Nkx2.5* inhibits ANF expression in the atrioventricular canal: implications for cardiac chamber formation. *Genes Dev.* **16**, 1234–1246.
- Herrmann, B. G., Labiet, S., Poustka, A., King, T. and Lehrach, H. (1990). Cloning of the *T* gene required in mesoderm formation in the mouse. *Nature* **343**, 617–622.
- Hiroi, Y., Kudoh, S., Monzen, K., Ikeda, Y., Yazaki, Y., Nagai, R. and Komuro, I. (2001). *Tbx5* associates with *Nkx2-5* and synergistically promotes cardiomyocyte differentiation. *Nat. Genet.* **28**, 276–280.
- Hoogaars, W. M. H., Tessari, A., Moorman, A. F. M., de Boer, P. A. J., Hagoort, J., Soufan, A. T., Campione, M. and Christoffels, V. M. (2004). The transcriptional repressor *Tbx3* delineates the developing central conduction system of the heart. *Cardiovasc. Res.* **62**, 489–499.
- Jacks, T., Remington, L., Williams, B. O., Schmitt, E. M., Halachmi, S., Bronson, R. T. and Weinberg, R. A. (1994). Tumor spectrum analysis in *p53*-mutant mice. *Curr. Biol.* **4**, 1–7.
- Jacobs, J. J. L., Keblusek, P., Robanus-Maandag, E., Kristel, P., Lingbeek, M., Nederlof, P. M., van Welsem, T., van de Vijver, M. J., Koh, E. Y., Daley, G. Q. et al. (2000). Senescence bypass screen identifies *TBX2*, which represses *Cdkn2a* (*p19^{ARF}*) and is amplified in a subset of human breast cancers. *Nat. Genet.* **26**, 291–299.
- Jegalian, B. G. and de Robertis, E. M. (1992). Homeotic transformations in the mouse induced by overexpression of a human *Hox3.3* transgene. *Cell* **71**, 901–910.
- Jerome, L. A. and Papaioannou, V. E. (2001). DiGeorge syndrome phenotype in mice mutant for the T-box gene, *Tbx1*. *Nat. Genet.* **27**, 286–291.
- Kaufman, M. H. and Bard, J. B. L. (1999). *The Anatomical Basis of Mouse Development*. San Diego, CA: Academic Press.
- Kelly, R. G., Brown, N. A. and Buckingham, M. E. (2001). The arterial pole of the mouse heart forms from *Fgf10*-expressing cells in pharyngeal mesoderm. *Dev. Cell* **1**, 435–440.
- Kirby, M. L. and Waldo, K. L. (1995). Neural crest and cardiovascular patterning. *Circ. Res.* **77**, 211–215.

- Kraus, F., Haenig, B. and Kispert, A. (2001a). Cloning and expression analysis of the mouse T-box gene *Tbx18*. *Mech. Dev.* **100**, 83-86.
- Kraus, F., Haenig, B. and Kispert, A. (2001b). Cloning and expression analysis of the mouse T-box gene *Tbx20*. *Mech. Dev.* **100**, 87-91.
- Lamolet, B., Pulichino, A.-M., Lamonerie, T., Gauthier, Y., Brue, T., Enjalbert, A. and Drouin, J. (2001). A pituitary cell-restricted T box factor, Tpit, activates POMC transcription in cooperation with Pitx homeoproteins. *Cell* **104**, 849-859.
- Lindsay, E. A., Vitelli, F., Su, H., Morishima, M., Huynh, T., Pramparo, T., Jurecic, V., Ogunrinu, G., Sutherland, H. F., Scambler, P. J. et al. (2001). *Tbx1* haploinsufficiency in the DiGeorge syndrome region causes aortic arch defects in mice. *Nature* **410**, 97-101.
- Lingbeek, M. E., Jacobs, J. J. L. and van Lohuizen, M. (2002). The T-box repressors *TBX2* and *TBX3* specifically regulate the tumor suppressor gene *p14^{ARF}* via a variant T-site in the initiator. *J. Biol. Chem.* **277**, 26120-26127.
- Liu, W. and Saint, D. A. (2002). A new quantitative method of real time reverse transcription polymerase chain reaction assay based on simulation of polymerase chain reaction kinetics. *Anal. Biochem.* **302**, 52-59.
- Lyons, G. E., Schiaffino, S., Sassoon, D., Barton, P. and Buckingham, M. (1990). Developmental regulation of myosin gene expression in mouse cardiac muscle. *J. Cell Biol.* **111**, 2427-2436.
- Mahlamaki, E. H., Barlund, M., Tanner, M., Gorunova, L., Hoglund, M., Karhu, R. and Kallioniemi, A. (2002). Frequent amplification of 8q24, 11q, 17q, and 20q-specific genes in pancreatic cancer. *Genes Chromosomes Cancer* **35**, 353-358.
- Mahlapuu, M., Ormestad, M., Enerback, S. and Carlsson, P. (2001). The forkhead transcription factor *Foxf1* is required for differentiation of extra-embryonic and lateral plate mesoderm. *Development* **128**, 155-166.
- Moorman, A. F. M. and Christoffels, V. M. (2003). Cardiac chamber formation: development, genes, and evolution. *Physiol. Rev.* **83**, 1223-1267.
- Nagy, A., Rossant, J., Nagy, R., Abramow-Newerly, W. and Roder, J. C. (1993). Derivation of completely cell culture-derived mice from early-passage embryonic stem cells. *Proc. Natl. Acad. Sci. USA* **90**, 8424-8428.
- Naiche, L. A. and Papaioannou, V. E. (2003). Loss of *Tbx4* blocks hindlimb development and affects vascularization and fusion of the allantois. *Development* **130**, 2681-2693.
- O'Brien, T. X., Lee, K. J. and Chien, K. R. (1993). Positional specification of ventricular myosin light chain 2 expression in the primitive murine heart tube. *Proc. Natl. Acad. Sci. USA* **90**, 5157-5161.
- Palmer, S., Groves, N., Schindeler, A., Yeoh, T., Biben, C., Wang, C.-C., Sparrow, D. B., Barnett, L., Jenkins, N. A., Copeland, N. G. et al. (2001). The small muscle-specific protein Csl modifies cell shape and promotes myocyte fusion in an Insulin-like Growth Factor 1-dependent manner. *J. Cell Biol.* **153**, 985-997.
- Papaioannou, V. E. (2001). T-Box genes in development: from hydra to humans. *Int. Rev. Cytol.* **207**, 1-70.
- Prince, S., Carreira, S., Vance, K. W., Abrahams, A. and Goding, C. R. (2004). *Tbx2* directly represses the expression of the p21^{WAF1} cyclin-dependent kinase inhibitor. *Cancer Res.* **64**, 1669-1674.
- Ramakers, C., Ruijter, J. M., Lekanne Deprez, R. H. and Moorman, A. F. M. (2003). Assumption-free analysis of quantitative real-time polymerase chain reaction (PCR) data. *Neurosci. Lett.* **339**, 62-66.
- Showell, C., Binder, O. and Conlon, F. L. (2004). T-box genes in early embryogenesis. *Dev. Dyn.* **229**, 201-218.
- Sinha, S., Abraham, S., Gronostajski, R. M. and Campbell, C. E. (2000). Differential DNA binding and transcription modulation by three T-box proteins, T, TBX1 and TBX2. *Gene* **258**, 15-29.
- Suzuki, T., Takeuchi, J., Koshiba-Takeuchi, K. and Ogura, T. (2004). *Tbx* genes specify posterior digit identity through Shh and BMP signaling. *Dev. Cell* **6**, 43-53.
- Tanaka, M., Chen, Z., Bartunkova, S., Yamasaki, N. and Izumo, S. (1999). The cardiac homeobox gene *Csx/Nkx2.5* lies genetically upstream of multiple genes essential for heart development. *Development* **126**, 1269-1280.
- Taylor, W. R. and Stark, G. R. (2001). Regulation of the G2/M transition by p53. *Oncogene* **20**, 1803-1815.
- Thomas, T., Yamagishi, H., Overbeek, P. A., Olson, E. N. and Srivastava, D. (1998). The bHLH factors, dHAND and eHAND, specify pulmonary and systemic cardiac ventricles independent of left-right sidedness. *Dev. Biol.* **196**, 228-236.
- Walther, T., Schultheiss, H.-P., Tschöpe, C. and Stepan, H. (2002). Natriuretic peptide system in fetal heart and circulation. *J. Hypertens.* **20**, 785-791.
- Wilkinson, D. G. (1992). *Whole Mount In Situ Hybridization of Vertebrate Embryos*. Oxford, UK: IRL Press.
- Yagi, H., Furutani, Y., Hamada, H., Sasaki, T., Asakawa, S., Minoshima, S., Ichida, F., Joo, K., Kimura, M., Imamura, S. et al. (2003). Role of *TBX1* in human del22q11.2 syndrome. *Lancet* **362**, 1366-1373.
- Yamada, M., Revelli, J.-P., Eichele, G., Barron, M. and Schwartz, R. J. (2000). Expression of chick *Tbx-2*, *Tbx-3*, and *Tbx-5* genes during early heart development: evidence for BMP2 induction of *Tbx2*. *Dev. Biol.* **228**, 95-105.
- Zindy, F., Quelle, D. E., Roussel, M. F. and Sherr, C. J. (1997). Expression of the p16^{INK4a} tumor suppressor versus other INK4 family members during mouse development and aging. *Oncogene* **15**, 203-211.